HHS Public Access

Author manuscript

Exp Eye Res. Author manuscript; available in PMC 2016 October 01.

Published in final edited form as:

Exp Eye Res. 2015 October ; 139: 1–12. doi:10.1016/j.exer.2015.05.011.

Rat Optic Nerve Head Anatomy within 3D Histomorphometric Reconstructions of Normal Control Eyes

Marta Pazos[a,d], **Hongli Yang**[a], **Stuart K. Gardiner**[b], **William O. Cepurna**[c], **Elaine C. Johnson**[c], **John C. Morrison**[c], and **Claude F. Burgoyne**[a]

[a]From the Devers Eye Institute, Optic Nerve Head Research Laboratory, Legacy Health System, Portland, Oregon

[b]Devers Eye Institute, Discoveries in Sight, Legacy Health System, Portland, Oregon

[c]Kenneth C. Swan Ocular Neurobiology Laboratory, Casey Eye Institute, Oregon Health and Science University, Portland, OR

[d]Hospital de l'Esperança. Parc de Salut Mar. Universitat Autònoma de Barcelona, Barcelona, Spain.

Abstract

The purpose of this study is to three-dimensionally (3D) characterize the principal macroscopic and microscopic relationships within the rat optic nerve head (ONH) and quantify them in normal control eyes. Perfusion-fixed, trephinated ONH from 8 normal control eyes of 8 Brown Norway Rats were 3D histomorphometrically reconstructed, visualized, delineated and parameterized. The rat ONH consists of 2 scleral openings, (a superior neurovascular and inferior arterial) separated by a thin connective tissue strip we have termed the “scleral sling”. Within the superior opening, the nerve abuts a prominent extension of Bruch's Membrane (BM) superiorly and is surrounded by a vascular plexus, as it passes through the sclera, that is a continuous from the choroid into and through the dural sheath and contains the central retinal vein (CRV), (inferiorly). The inferior scleral opening contains the central retinal artery and three long posterior ciliary arteries which obliquely pass through the sclera to obtain the choroid. Bruch's Membrane Opening (BMO) is irregular and vertically elongated, enclosing the nerve (superiorly) and CRV and CRA (inferiorly). Overall mean *BMO Depth*, *BMO Area*, *Choroidal Thickness* and peripapillary *Scleral Thickness* were 29 μm, 56.5 × 10^3 μm^2, 57 μm and 104 μm respectively. Mean anterior scleral canal opening (*ASCO)* and posterior scleral canal opening (*PSCO)* radii were 201 ± 15 μm and 204 ± 16 μm, respectively. Mean optic nerve area at the ASCO and PSCO were 46.3 × 10^3 ± 4.4 × 10^3 μm^2 and 44.1 × 10^3 ± 4.5 × 10^3 μm^2 respectively. In conclusion, the 3D complexity of the rat ONH and the extent to which it differs from the primate have been under-appreciated within previous 2D

Corresponding Author: Claude F. Burgoyne, MD, Devers Eye Institute, Optic Nerve Head Research Laboratory, 1225 NE 2nd Ave, Portland OR 97232. cfburgoyne@deverseye.org. Tel: +1-503-413-5441 Fax: +1-503-413-5179.

Marta Pazos and Hongli Yang are co-first authors of this work.

studies. Properly understood, these anatomic differences may provide new insights into the relative susceptibilities of the rat and primate ONH to elevated intraocular pressure.

Keywords

Glaucoma; Rat; Optic Nerve Head; Neural Canal; Scleral Canal; Optic Nerve

1. Introduction

Nonhuman primate (NHP) experimental glaucoma is a well-established animal model for studying human glaucoma in part because the NHP optic nerve head (ONH) shares a close anatomic association with the human ONH. However, these animals are impractical for studies that require large animal numbers and at present cannot easily be genetically manipulated. For these and other reasons, mouse and rat (Dai et al., 2012; Howell et al., 2007; Johnson and Tomarev, 2010; Mabuchi et al., 2003, 2004; May, 2008; Morrison et al., 2011; Morrison et al., 2008; Pang and Clark, 2007; Ruiz-Ederra and Verkman, 2006) experimental glaucoma models are increasingly utilized to study the mechanisms of chronic intraocular pressure-induced optic nerve head (ONH) and retinal ganglion cell (RGC) axon injury.

The anatomy of the rodent ONH is widely recognized to differ from the human and non-human primate (Dai et al., 2012; Morrison et al., 2011; Morrison et al., 1999; Sugiyama et al., 1999). Post mortem, histologic measurements in fixed and processed tissues suggest that the rat eye is approximately 6.29 mm in axial length and 6.41 mm in diameter, with a posterior sclera that is about 5 to 10 times thinner and a circular scleral canal that is about 4 times smaller than the human eye. Normal rat optic nerve axon counts range from 0.11 to 0.14 million axons compared to 1.2 to 2.0 million in the human eye and from 0.9 to 1.4 million in monkeys. Reported differences in normal rat ONH anatomy include a lack of a well-defined collagenous lamina cribrosa, a cellular lamina-like structure formed by sparse connective tissue associated with blood vessels lined with astrocytes (Dai et al., 2012; Li et al., 2015) and composed of extracellular matrix materials which are themselves similar to those within the primate lamina cribrosa (Fujita et al., 2000; Johansson, 1987; Morrison et al., 1995a; Morrison et al., 2011), a perineural vascular plexus that surrounds the optic nerve within the scleral canal (Morrison et al., 1999; Sugiyama et al., 1999) and an ophthalmic artery (OA) that splits just posterior to the globe into the central retinal artery (CRA) and three long posterior ciliary arteries (LPCAs) (Morrison et al., 1999; Sugiyama et al., 1999). All previous characterizations of the rat ONH have been based upon traditional histologic sections or 2D photos of 3D vascular casts. These studies have therefore lacked the ability to digitally sample and visualize the same reconstruction from multiple viewpoints at the same time so as to confront, understand and characterize its principal organizing relationships.

The purpose of the present study was to perform high-resolution (1.5 μm × 1.5 μm × 1.5 μm voxel) 3D histomorphometric reconstruction of the ONH and peripapillary scleral trephines of 8 normal control eyes of 8 Brown Norway rats so as to describe and quantify the important macroscopic and microscopic morphologic relationships. Our conceptual

framework for organizing the anatomy of the rat ONH is explained in Figs. 1 and 7. These concepts are necessary to understand the logic of our measurement parameters which are explained in Appendix Figs. 1–4. Table 1 is a reference for all abbreviations. In this report we present data on the contralateral "normal" control eyes of 8 rats that were given unilateral experimental glaucoma (EG) in one eye. In a, follow-up study we will use similar techniques to test hypotheses about how these relationships will change in early rat EG.

2. Materials and Methods

2.1 Animals and eyes

All animals were treated in accordance with the ARVO Statement for the Use of Animals in Ophthalmic and Vision Research. Eight normal control eyes of 8 male Brown Norway rats, between 9.5 and 10.5 months of age, were studied (Table 2) under constant light conditions for this report. Eye-specific mean IOP (by TonoPen testing (Moore et al., 1995; Moore et al., 1993; Morrison et al., 2009)) for the 8 eyes of this study was within the normal range of our previous reports for animals under constant light (Johnson et al., 2015; Johnson et al., 1996; Moore et al., 1996; Morrison, 2005; Morrison et al., 2005; Pang and Clark, 2007). These eyes represent the normal control eyes of 8 rats that had undergone 4 weeks of unilateral chronic IOP elevation following hypertonic saline treatment (Jia et al., 2000; Morrison et al., 1997) to the trabecular meshwork of the contralateral study eye. A follow up report, will describe the changes in the 8 early EG eyes of these same animals, however, a delineation reproducibility study, described below, was performed in both eyes of each animal.

2.2 Rat Euthanasia and Fixation

All animals were sacrificed under isoflurane anesthesia by transcardial injection (1 ml/kg) of heparin (1000U/ml) containing 10 mg/ml sodium nitroprusside followed by 1 liter of 5% glutaraldehyde in 0.1 M phosphate buffer (pH 7.2).

2.3 3D Histomorphometric Reconstruction of the ONH

(Burgoyne et al., 2004; Downs et al., 2007; Yang et al., 2007a; Yang et al., 2007b; Yang et al., 2009b; Yang et al., 2011). The ONH and peripapillary sclera of each eye were trephined (3-mm-diameter), embedded in paraffin, mounted to a microtome (RM2165; Leica, Wetzlar, Germany) and serial sectioned at 1.5 μm thickness from the vitreous surface through the optic nerve head into the orbital optic nerve (Burgoyne et al., 2004). After each section was cut, the block surface was stained with a 1:1 (v/v) mixture of Ponceau S and acid fuchsin stains, then imaged at a resolution of 1.5 × 1.5 μm per pixel using a custom device (Burgoyne et al., 2004). For each ONH 275 to 501 serial digital transverse section images were thus generated, aligned and stacked into a digital 3D reconstruction (Burgoyne et al., 2004; Downs et al., 2007; Yang et al., 2007a; Yang et al., 2007b; Yang et al., 2009b; Yang et al., 2011).

2.4 Initial Qualitative 3D Visualization of each ONH reconstruction and comparison to existing light and electron microscopy

To gain an initial understanding of the anatomy (Figures 1 and 2) and to design a landmark and parameterization scheme appropriate to the rat ONH (Appendix Figures 1-4), 40 radial digital sagittal sections from each ONH reconstruction (Figure 3A and 3B) were viewed by the authors (as a group) using our custom Multiview 3D visualization software (based on the Visualization Toolkit [VTK], Clifton Park, NY) (Burgoyne et al., 2004; Downs et al., 2007; Morrison et al., 1999; Yang et al., 2007a; Yang et al., 2007b; Yang et al., 2009b). Where indicated, selected comparisons were made to existing stained histologic sections, electron micrographs and vascular casting photographs from normal rat eyes that had been studied as part of a series of previous reports(Morrison et al., 2011; Morrison et al., 1995b; Morrison et al., 2005; Morrison et al., 1997). With the basic macroscopic and microscopic relationships thus established (Figures 1 and 2), strategies for delineation (Figures 3 and 4) and parameterization (Appendix Figures 1-4) were developed and executed. Final qualitative 3D visualization of the delineated point clouds (Figures 3-7) were then performed to confirm the anatomic relationships described herein.

2.5 3D Delineation of the ONH and Peripapillary Scleral Landmark Points (Figure 3)

(Downs et al., 2007; Yang et al., 2007b; Yang et al., 2011) Each 3D ONH reconstruction was loaded into Multiview memory and the delineator assigned the approximate center of the optic nerve (Figures 2 and 3) as the center of rotation, through which, forty, 7-voxel thick, digital radial sagittal slices of the digital 3D reconstruction were serially served at 4.5° intervals for delineation (Figure 3A, B and C). Because visualization of Bruch's Membrane (BM), Bruch's Membrane Opening (BMO) and several deep ONH landmarks was most consistent within Green channel as opposed to white light section images, delineation was carried out within green channel digital section images for each study eye. Four landmark surfaces and three pairs of neurovascular canal landmarks (one point on each side of the canal) were delineated within each digital section image. The landmark surfaces were: (1) BM; (2) the anterior and (3) posterior surfaces of peripapillary sclera; and (4) the optic nerve boundary extending from BMO, through the neurovascular scleral canal and along the pia mater to the posterior edge of the reconstruction (Figure 3B). The landmark points were BMO, the anterior scleral canal opening (ASCO) and the posterior scleral canal opening (PSCO).

Delineation of these landmarks was “three dimensional” because while marking the digital sagittal section image (Figure 3B), the delineator simultaneously viewed a second window, (that was linked to the first), displaying the cursor's real-time 3D location within the appropriate digital transverse section image (Figure 3A). The 3D Cartesian coordinates and category number for each mark were saved, generating a 3D point cloud representing each of the marked structures (Figure 3D). These point clouds were then surfaced and could themselves be cut and visualized at any angle allowing observations and measurements to be made between the regions of actual delineation.

2.6 3D Delineation of the ONH and Peripapillary Scleral Vasculature and Scleral Sling (Figure 4)

(Downs et al., 2007; Yang et al., 2007b; Yang et al., 2011) As opposed to the landmark and surface delineations outlined above which were performed within serial digital sagittal section images (Figure 3), vessel and scleral sling delineation were performed within every fourth digital transverse section image while simultaneously viewing linked windows which displayed vertical or horizontal digital sagittal sections (notice this is not clinical vertical or horizontal sections due to our embedding angles) of the reconstruction through the point being delineated (Figure 4A–D). The following landmark categories were individually marked and catalogued within each delineated transverse section image: (1) Ophthalmic artery (OA); (2) central retinal artery (CRA); (3) long posterior ciliary arteries (LPCAs); (4) short posterior ciliary arteries (SPCAs); (5) Central retinal vein (CRV); and (6) the vascular or neural boundary of the scleral sling (Figures 1, 2 and 4). Three dimensional reconstructions of the landmark point clouds (Figures 4E–H and Figure 5) were then visualized together and separately (turning each landmark category on and off) so as to determine their principal macroscopic relationships.

2.7 Delineation Reproducibility Study

Both the normal and experimental glaucoma eye of each animal were delineated by a single delineator (MP). Upon completion of the initial delineation of each eye, the marks were reviewed by 2 senior authors (CFB and HY) to expand our understanding of the anatomy and to reach agreement on the anatomic landmarks of greatest interest. Both eyes of three animals were then delineated on two subsequent occasions by the same delineator (MP), at least 2 weeks apart, to assess intra-delineator variability. The Intraclass-Correlation Coefficient (ICC) (see statistical analysis, below) for all reported parameters were calculated (Rosner, 2011).

2.8 Parameterization and Quantification

Parameters are italicized to distinguish their behavior from the behavior of the underlying anatomic landmarks (which are not italicized).

2.9 Bruch's Membrane Opening (BMO) and the Neurovascular Scleral Canal (Appendix Figures 1 and 2)

For each ONH reconstruction, individual planes were fit to the 80 BMO points, 80 neurovascular ASCO points and 80 neurovascular PSCO points, (2 points for each landmark within each of 40 digital radial sagittal sections, as outlined above (Appendix Figures 1A)) using a least-squares algorithm. The BMO plane became the reference plane for a series of subsequent measurements and the basis for the second peripheral anterior scleral reference plane (Appendix Figures 1A, 2 and 3). The cross-sectional area of BMO (*BMO Area*) as well as the neurovascular sclera canal at the level of the ASCO and PSCO (*ASCO* and *PSCO area*) were calculated as the area within the projection of the BMO, ASCO and PSCO points to their respective fitted planes (Appendix Figure 1B). Using the centroid of the projected BMO, ASCO and PSCO points, 80 radius measurements were made within their respective

fitted planes at 4.5 degree intervals (Appendix Figure 1C). To assess their relative shapes, the *Horizontal/Vertical (H/V) Diameter Ratios* were calculated for ASCO, and PSCO.

2.10 Optic Nerve cross-sectional area within the scleral canal (Appendix Figure 2)

Optic nerve (ON) cross-sectional area, radii and shape (*H/V Diameter Ratios)* were quantified within the ASCO (*ON-ASCO*) and PSCO (*ON-PSCO*) planes using the delineated optic nerve boundary as illustrated in Appendix Figure 2. *Optic Nerve Volume* (the volume defined by the ASCO plane, PSCO plane and optic nerve boundary) was also quantified.

2.11 *Anterior Scleral Sling Depth, BMO/ASCO/PSCO Depth*, and *Anterior Peripapillary Scleral Surface Depth* Relative to a Peripheral Anterior Scleral Reference Plane (Appendix Figure 3)

BMO Depth, ASCO Depth, PSCO Depth (Appendix Figure 3C) were separately measured relative to a peripheral anterior scleral reference plane (Appendix Figure 3A) within each digital sagittal section image as illustrated in Appendix Figures 3B and 3C. *Anterior Peripapillary Scleral Depth* was measured relative to the same reference plane commencing at 350 μm and extending to 700 μm from the projection of the ASCO centroid line (in 50μm increments) as illustrated in Appendix Figure 3D. These distances were chosen because this was a region of sclera that was common to all studied eyes (i.e. 350 μm corresponded to the smallest radius and 700 μm the largest radius from the centroid of ASCO that included sclera for all 360 degrees within each of the 8 rat volumes).

2.12 *Peripapillary Scleral* and *Peripapillary Choroidal Thickness* (Appendix Figure 4)

Peripapillary Scleral and *Choroidal Thickness* were separately measured within each digital sagittal section image in 50 μm increments radially commencing at 350 μm and extending to 700 μm (*Peripapillary Scleral Thickness*) or 600 μm (*Peripapillary Choroidal Thickness*) from the projection of the ASCO centroid onto the BMO reference plane as illustrated in Appendix Figure 4. Again 350 μm corresponded to the smallest radius outside the major vessels and 600 or 700 μm (depending on the parameter) was the largest radius present in all the specimens.

2.13 The Inferior Arterial Scleral Opening

Because its boundaries are not consistently clearly visible we were not able to quantify the inferior opening in the sclera created by the central retinal artery, the LPCAs and the LPCA intrascleral branches using our current techniques.

2.14 Statistical Analysis

Mixed effects linear regression models were formed to compare the radial structures (ASCO radius vs PSCO radius, ON-ASCO radios vs ON-PSCO radius). Within each rat, anterior and posterior scleral and neural canal sizes were compared using a linear model fitted with generalized least squares (GLS). To assess consistency or reproducibility of the quantitative measurements made in different days measuring the same parameters, the ICC was calculated from one-way ANOVA(Rosner, 2011). When multiple measurements within an eye were not present (*ASCO area*, *PSCO area*) a linear regression was performed. ANOVA

using linear mixed effect model was used to determine whether there was an overall regional effect. A secondary analysis was carried out to compare the quadrant with the lowest value to the rest of other three quadrants. Statistical significance was defined to occur at $p<0.05$ after adjusted to multiple comparisons. Analysis was performed either in R (the R Foundation for Statistical Computing, Vienna, Austria) or Microsoft Excel (Microsoft, Redmond, WA, USA).

3. Results

Animal demographic data are reported in Table 2.

3.1 Principal Macroscopic and Microscopic Relationships

The rat optic nerve head consists of two principal passages through the sclera (Figures 1, 2, 3, 4 and 5): a well demarcated superior neurovascular canal that contains the optic nerve and its peri-neural vascular plexus (continuous with and extending from the choroid to the dural sheet veins and containing the CRV, inferiorly) and a less clearly defined, more-inferior arterial opening through which pass the CRA, LPCAs and their intrascleral branches to the peripapillary choroid. The connective tissue wall of these two openings and the outer walls of the vessels that pass through them fuse with a sling of scleral connective tissues to form a separating structure that we have called the *scleral sling.*

Figures 1 and 2 describe these relationships in 2 dimensions and Figures 3-7 utilize the 3D point clouds of the delineated landmarks from a representative rat ONH to emphasize the following features. First, at the level of BMO, BM extends prominently beyond the scleral canal opening (Figures 2, 5 and 6) superiorly to physically abut the RGC axon bundles, (Figure 5) while both the CRV and CRA physically separate the RGC axons from BMO inferiorly (Figure 5). The fact that the CRA passes through the sclera inferior to the neurovascular canal (within its own opening) but joins the CRV within the inferior portion of BMO, leaves BMO irregularly shaped with an inferior elongation that is not present in the primate eye (Figures 5 and 6).

Second, at the level of the sclera, also unlike the primate, there is a prominent vascular plexus between the neural tissue and the ASCO and PSCO in Figures 2B and 3B. Within the scleral portion of the neurovascular canal there were sporadic organized connective tissue structures within our reconstructions; however no clear evidence of laminar beams were observed using our technique. Also unlike the primate in which the shape of the optic nerve as it passes through the sclera ranges from circular to a vertical ellipse, in the rat eye, the optic nerve passes through the neurovascular scleral canal as a horizontal, kidney bean-like ellipse, with the ratio of horizontal to vertical diameter varying from 1.66 to 2.18 in these 8 normal ONH (see the quantitative results, below).

Third, there are 3 LPCAs which branch from the CRA behind the globe and pass (together with the CRA) through the sclera inferior to the neurovascular canal to achieve the choroid (Figures 1, 2, 4, 5 and 7). Their tangential rather than perpendicular passage through the sclera is depicted in Figure 7 in which the anterior and posterior scleral point clouds have been surfaced so as to enhance LPCA and scleral visualization. Fourth, short posterior

ciliary arteries (SPCA) - defined to be primary branches of the ophthalmic artery that individually pass through the sclera do not appear to exist in the rat eye. While there appear to be a few arteries that independently pass through the sclera superiorly (Figure 5G), where identified, these seem to be retrobulbar branches of the LPCAs. Fifth, unlike the primate eye in which there are approximately 15 SPCAs (Sugiyama et al., 1994) that are relatively equidistant from one another around the circumference of the optic nerve and follow a relatively perpendicular course through the sclera, the choroidal blood supply in the rat appears to originate inferiorly from a dense plexus of tangentially running, intrascleral LPCA branches which effectively fill the space between the three LPCA branches and the CRA. Some of these vessels extend within the sclera and choroid superiorly, around the neurovascular canal. It is the density of the LPCAs and their intrascleral branches inferiorly that does not allow the sclera between them to be discerned. Thus, unlike the neurovascular scleral opening which is regular enough to call a canal, the borders of the inferior arterial opening are highly irregular, preventing quantitative parameterization of this opening by our method.

Sixth, within the sclera, and prior to their intertwining within the inferior notch of BMO, the CRA and CRV are separated by a “sling” of scleral tissues (the scleral sling) which forms the inferior border of the neurovascular scleral canal opening and the superior border of the more-inferior arterial opening (Figures 1, 2, 4, and 5).

3.2 Principal Quantitative Results

3.2.1 Reproducibility—Reproducibility was excellent (ICC values greater than 0.75 (Appendix Table 1)) or fair to good (ICC 0.5 - 0.75) for all parameters(Rosner, 2011).

3.2.2 Parameters treated globally—The eye-specific means and standard deviations (SDs) for our global parameters are reported in Appendix Tables 1-4.

3.2.2.1 BMO Size (Appendix Table 2): Eye-specific *BMO Area* ranged from 4.76×10^4 to 6.90×10^4 μm^2 with an overall mean of $5.65\times10^4 \pm 0.66\times10^4$ μm^2. *Eye-specific mean BMO Radii* ranged from 122 ± 14 to 148 ± 8 μm, with an overall mean of 133 ± 8 μm.

3.2.2.2 The Neurovascular Scleral Canal (Appendix Table 3): *PSCO Area* ($1.33 \times 10^5 \pm 0.21 \times 10^5$ μm^2) was greater than *ASCO Area* ($1.29 \times 10^5 \pm 0.19 \times 10^5$ μm^2) overall but this difference was not significant. Since there is a vascular plexus surrounding the nerve, which includes the CRV inferiorly, *ASCO* and *PSCO Areas* and *Radii* were larger than those of the neural tissues themselves (*ON-ASCO* and *ON-PSCO Areas* and *Radius* values, respectively). Mean *ASCO* and Mean *PSCO Area* were 2.8 and 3.0 times greater than Mean *ON-ASCO* and Mean *ONPSCO Area*, respectively. PSCO Radius (204 ± 16 μm) was similar to ASCO Radius, (201 ± 15) μm overall, but this difference did not achieve significance. However, eye-specific mean PSCO radius was significantly larger than mean ASCO radius in four animals (Rats 3, 4, 6, and 7, $p < 0.05$, GLS method). Eye-specific *ASCO* and *PSCO H/V Diameter Ratios* ranged from 1.11 to 1.42 (ASCO) and 1.10 to 1.47 (PSCO) respectively confirming the horizontal orientation of the long axis of the ellipse in all 8 eyes.

3.2.2.3 The Optic Nerve Within the Neurovascular Scleral Canal (Appendix Table 4): *ON-ASCO Area* was very similar to *ON-PSCO Area* both overall (means $4.63 \times 10^4 \pm 0.44 \times 10^4$ μm^2 vs $4.41 \times 10^4 \pm 0.45 \times 10^4$ μm^2) and within each animal ($p > 0.05$). Eye-specific ON-*ASCO H*/*V Diameter Ratios* ranged from 1.66 to 2.18 and ON-*PSCO H*/*V Diameter Ratios* ranged from 1.81 to 2.97, respectively. Eye-specific *ON Volume* ranged from 2.29×10^6 to 4.04×10^6 μm^3 with an overall mean of $3.28 \times 10^6 \pm 0.59 \times 10^6$ μm^3.

3.2.2.4 *BMO Depth*, *ASCO Depth*, *PSCO Depth* and *Anterior Peripapillary Scleral Surface Depth* relative to a peripheral anterior scleral reference plane (Appendix Table 4): Eye-specific *BMO Depth* relative to a peripheral anterior scleral reference plane (Figure 7C) ranged from −1 ± 5 to 47 ± 9 μm (overall mean of 29 ± 15 μm). Eye-specific *Anterior Peripapillary Scleral Surface Depth* relative to the same reference plane (Fig. 7D) ranged from 19 ± 23 to 39 ± 29 μm (overall mean of 33 ± 7 μm).

3.2.2.5 *Peripapillary Scleral* and *Choroidal Thickness* (Appendix Table 5): Eye-specific *Peripapillary Scleral Thickness* ranged from 97 ± 23 to 110 ± 18 μm. *Peripapillary Choroidal Thickness* ranged from 45 ± 11 to 70 ± 26 μm.

3.2.3 Parameters treated regionally—Appendix Table 6 reports overall regional values for the subset of parameters which include multiple measurements per region. Regional effects were significant ($p < 0.05$ ANOVA) for ASCO Radius, PSCO Radius, ON-ASCO radius, ON-PSCO radius, Scleral Thickness and Scleral Depth. Among these parameters, *scleral thickness* was significantly thinner within the inferior quadrant, and *scleral depth* was significantly shallower in the temporal quadrant compared to all other quadrants. ASCO Radius, PSCO Radius, ON-ASCO and ON-PSCO radius were smallest within the inferior quadrant.

4. Discussion

The principal findings of this study are as follows. First, while the rat ONH is built around a well-defined neurovascular scleral canal that contains the retinal ganglion cell axon bundles surrounded by a vascular plexus that includes the CRV, we believe that the density of the more-inferior CRA and LPCA passageways through the sclera effectively constitute a second, arterial scleral opening that is less well defined and separated from the neurovascular scleral opening by a thin connective tissue band we have named the scleral sling. Second, at the level of BMO, BM extends prominently beyond the scleral canal opening superiorly to physically abut the RGC axon bundles, while inferiorly, the CRV and CRA physically separate the RGC axons from BMO. Third, the fact that the CRA passes through the sclera inferior to the neurovascular canal (within its own opening) but joins the CRV within the inferior portion of BMO, leaves BMO irregularly shaped with an inferior elongation that is not present in the primate eye. Fourth, within the neurovascular canal, at the level of the sclera, the retinal ganglion cell axons are bundled into a nerve that is surrounded by a vascular plexus in a manner that leaves its physical attachments to the surrounding sclera impossible to discern by our method (see discussion below). This plexus appears to be a continuation of the choroid that ultimately drains into the retrobulbar pial and dural sheaths. Fifth, the three branches of the LPCAs densely and obliquely penetrate

the peripapillary sclera inferior to the neurovascular canal to obtain and run within the peripapillary choroid. Apart from the creation of an effective second opening in the sclera (as mentioned above) these LPCAs along with their dense intrascleral branches that pass to the superior choroid (similar to but less complete than the primate circle of Zinn-Haler) appear to be the principal source of blood supply to the choroid. In fact we found no evidence for SPCAs (defined to be separate branches of the Ophthalmic Artery) in these reconstructions.

This is the first description of the rat ONH that defines it to consist of two separate passage ways through the sclera separated by a thin connective tissue strip (that we have termed the scleral sling). While the biomechanical implications of this anatomy remain to be determined, the large and irregular inferior arterial passageway (containing the CRA, the LPCAs and their intrascleral branches) combined with the lack of SPCAs, are two conditions that do not exist in the primate eye.

While the prominent superior extension of BM has not previously been noted, it is easily visualized within Spectral Domain Optical Coherence Tomographic B-scans (verbal communication, Brad Fortune). The superior location of RGC axon interaction with BMO has previously been described by light microscopy (Morrison et al., 2011; Morrison et al., 2008). The fact that the retinal ganglion cell axons are surrounded by a vascular plexus within the neurovascular canal and that this plexus is at least regionally continuous with the peripapillary choroid has been noted by a series of previous investigators (Dai et al., 2012; Morrison et al., 1999; Sugiyama et al., 1999). In longitudinal sections from both studies (similar to Figure 2, panels B and F in this report) clear continuity between the choroid and the peri-neural vascular plexus can be appreciated. This vascular plexus does not exist in the primate and is difficult to examine with our method due to the heavy pigmentation contained therein.

In the primate, the peripapillary sclera and scleral canal wall connective tissues are thought to govern the distribution of IOP-related stress and strain within the lamina cribrosa connective tissues (Burgoyne and Downs, 2008; Sigal et al., 2005). Given the lack of a detectible connective tissue lamina and connective tissue connections between the nerve and the sclera, by our technique, the question of how the sclera transfers load to the retinal ganglion cell axons and the astrocytes that span the nerve within the canal is of substantial biomechanical interest. Two recent papers have described the relationship between the radially arrayed, rat optic nerve head astrocytes, the optic nerve pial sheath (a continuation of the pia that merges with Bruch's Membrane at its opening) and this vascular plexus (Dai et al., 2012; Li et al., 2015). Their description of the plexus suggests that it contains dense connective tissue septa. If these septa directly or indirectly span the plexus to link the sheath and the sclera, then they may be the means by which the sclera transfers IOP-related load to the ONH astrocytic array. The geometry and material properties of these cells, the sheath, and these septal connections to the sclera, thus require further study.

Regarding our quantitative results, previous studies (Downs et al., 2007; Yang et al., 2009a; Yang et al., 2009b; Yang et al., 2011) in a total of 21 normal eyes of 21 monkeys suggest that the mean rat *BMO Area* and mean rat BMO radii we report are 4.7% and 23%

(respectively) that of the monkey. In humans, Ren et al(Ren et al., 2009) used a post-mortem, 2-D technique within histologic sections to report mean BMO diameter that suggest the *BMO Radii* data we report appear to be approximately 17% the size of the human eye. Recently, using Spectral-Domain (SD) OCT in 48 healthy humans, Chauhan and colleagues reported a BMO Area of 1.7 mm^2 (1.4-1.9) which is about 30 times larger than the rat eye (Chauhan et al., 2013).

Like the (single) scleral canal in the primate, the neurovascular scleral canal in the rat expands within the sclera in half of the rat eyes. Interestingly, a study performed using en face Optical Coherence Tomography reported in vivo, OCT-detected ASCO diameter values of approximately 665 μm in 18 normal Dark Agouti rats (Guo et al., 2005). While tissue shrinkage due to fixation, embedding and species difference (estimated to be as high as 30%) (Abramson et al., 2003) may explain these differences, the in vivo study did not clarify the orientation of their measurements (long versus short axis of the horizontal ellipse), nor did it detect the elliptical (rather than circular) shape of this opening as we have herein described. In a post-mortem histologic study of 6 normal human ONHs, (Sigal et al., 2010) ASCO radius was 1.2 times larger than the monkey and 4 times larger than the rat eye.

Finally, because the manner in which mean scleral thickness measurements were made in rats was different from previous measurements made by us in monkeys (Burgoyne et al., 2004; Downs et al., 2007; Yang et al., 2007a; Yang et al., 2007b; Yang et al., 2009b; Yang et al., 2011), and others in humans (Ren et al., 2009; Sigal et al., 2010), direct comparison to the literature is not straightforward. Our data suggest that monkey peripapillary scleral thickness is 2 to 4 times thicker than that of the rat when compared at a similar eccentricity to the PSCO. Studies in human eyes (Norman et al., 2010; Ren et al., 2009; Sigal et al., 2010), which are not well matched to the location of measurement in our study, together suggest that human peripapillary sclera is profoundly thicker than that of the rat.

The limitations of our method of 3D reconstruction have been discussed previously(Burgoyne et al., 2004) and include: (1) anterior-to-posterior resolutions limited to 1.5 μm by the fact that the current stain penetrates approximately 1.5 μm into the block; (2) the stain is applied by hand to the block face with a cotton-tipped swab, and the excess is manually removed with lens paper, and thus staining variation between section images can be substantial; (3) there are tissue shrinkage effects (both from fixation and embedding) associated with this technique that may be unique to the rat eye and different within each constituent tissue of the ONH; and (4) the dense pigmentation of the rat vascular plexus surrounding the nerve may lead to an overestimation of ASCO and PSCO especially in the temporal/superior quadrants, due to the bending of the nerve; (5) Comparisons to our nonhuman primate and human cadaver eye data may be similar since post-tissue processing is similar, but comparisons to other post-mortem or in-vivo measurements may be affected by these differences; (6) Delineations were made using the approximate center of the ON as the point of rotation and the radial measurements were made from the centroids based on those delineations. The delineator's estimate of the ON center, and the fact that it was not necessarily the center of other ONH structures, may have influenced the regional sampling of the data.

Finally, it is possible that normal control eyes from unilateral EG animals raised in constant light environments, may not be identical to naive normal control eyes from bilaterally normal animals raised in the usual 12 hour light / dark cycle. However, there are no descriptions of normal control eye alteration in the rat unilateral EG model and none of the 8 normal control eyes in this study were found to have detectible alterations in their optic nerve axons by 2 graders masked to the status of each eye. While we do not believe that the morphologic relationships we describe will be different in naive status of raised in 12 hour light / dark conditions, the generalization of our quantitative findings to naïve normal eyes of all ages, rat strain and lighting conditions must be the subject of future studies.

In summary, we have performed the first 3D characterization of the macroscopic and microscopic ONH anatomy of the rat eye. Our study is the first to describe the rat ONH as consisting of two scleral openings and clarify that the CRA does not accompany the CRV within the neurovascular canal, but passes through a separate, large, irregular opening, inferior to it, accompanied by the LPCAs and their dense intra-scleral branches. Our findings confirm the presence of a vascular plexus that is continuous from the choroid to the optic nerve sheathes and surrounds the optic nerve within the neurovascular canal. We describe an anatomic proximity between the RGC axon bundles and a prominent extension of BM superiorly that is unique to that region. These data suggest that the rat ONH is remarkably different from the primate ONH. We propose that similar studies are now needed in the mouse and that inter-species differences will provide new insights into ONH susceptibility to glaucomatous damage in each species. Finally, we have used the same techniques described herein to study changes in the contralateral early EG eyes of these same 8 animals. The results of this study will be the subject of a future report.

Supplementary Material

Refer to Web version on PubMed Central for supplementary material.

Acknowledgments

The authors gratefully acknowledge the following individuals for their assistance with this study. Jonathan Grimm and Juan Reynaud for their assistance with software for volumetric and thickness quantification, Brad Fortune, Carla Abbott and Ross Ethier for their careful review of the manuscript and data interpretation, and Galen Williams and Christy Hardin for their performance of the serial section staining and imaging.

Supported in part by NIH grants R01EY011610 (CFB), R01EY10145 (JCM) and R01EY16866 (ECJ)) from the National Eye Institute, National Institutes of Health, Bethesda, Maryland; The Legacy Good Samaritan Foundation, Portland, Oregon; the Sears Trust for Biomedical Research, Mexico, Missouri; the Alcon Research Institute, Fort Worth, Texas; and an unrestricted grant from Research to Prevent Blindness.

REFERENCES

Abramson DH, et al. Optic nerve tissue shrinkage during pathologic processing after enucleation for retinoblastoma. Arch Ophthalmol. 2003; 121:73–75. [PubMed: 12523888]

Burgoyne CF, Downs JC. Premise and prediction-how optic nerve head biomechanics underlies the susceptibility and clinical behavior of the aged optic nerve head. J Glaucoma. 2008; 17:318–328. [PubMed: 18552618]

Burgoyne CF, et al. Three-dimensional reconstruction of normal and early glaucoma monkey optic nerve head connective tissues. Invest Ophthalmol Vis Sci. 2004; 45:4388–4399. [PubMed: 15557447]

Chauhan BC, et al. Enhanced detection of open-angle glaucoma with an anatomically accurate optical coherence tomography-derived neuroretinal rim parameter. Ophthalmology. 2013; 120:535–543. [PubMed: 23265804]

Dai C, et al. Structural basis of glaucoma: the fortified astrocytes of the optic nerve head are the target of raised intraocular pressure. Glia. 2012; 60:13–28. [PubMed: 21948238]

Downs JC, et al. Three-dimensional histomorphometry of the normal and early glaucomatous monkey optic nerve head: neural canal and subarachnoid space architecture. Invest Ophthalmol Vis Sci. 2007; 48:3195–3208. [PubMed: 17591889]

Fujita Y, et al. Comparative study of the lamina cribrosa and the pial septa in the vertebrate optic nerve and their relationship to the myelinated axons. Tissue Cell. 2000; 32:293–301. [PubMed: 11145012]

Guo L, et al. En face optical coherence tomography: a new method to analyse structural changes of the optic nerve head in rat glaucoma. Br J Ophthalmol. 2005; 89:1210–1216. [PubMed: 16113384]

Howell GR, et al. Axons of retinal ganglion cells are insulted in the optic nerve early in DBA/2J glaucoma. J Cell Biol. 2007; 179:1523–1537. [PubMed: 18158332]

Jia L, et al. Patterns of intraocular pressure elevation after aqueous humor outflow obstruction in rats. Invest Ophthalmol Vis Sci. 2000; 41:1380–1385. [PubMed: 10798653]

Johansson JO. The lamina cribrosa in the eyes of rats, hamsters, gerbils and guinea pigs. Acta Anat (Basel). 1987; 128:55–62. [PubMed: 3825488]

Johnson EC, et al. Radiation pretreatment does not protect the rat optic nerve from elevated intraocular pressure-induced injury. Invest Ophthalmol Vis Sci. 2015; 56:412–419. [PubMed: 25525172]

Johnson EC, et al. The effect of chronically elevated intraocular pressure on the rat optic nerve head extracellular matrix. Exp Eye Res. 1996; 62:663–674. [PubMed: 8983948]

Johnson TV, Tomarev SI. Rodent models of glaucoma. Brain Res Bull. 2010; 81:349–358. [PubMed: 19379796]

Li Y, et al. An energy theory of glaucoma. Glia. 2015 First published on Mar 23, 2015 as doi:10.1002/glia.22825.

Mabuchi F, et al. Optic nerve damage in experimental mouse ocular hypertension. Invest Ophthalmol Vis Sci. 2003; 44:4321–4330. [PubMed: 14507876]

Mabuchi F, et al. Regional optic nerve damage in experimental mouse glaucoma. Invest Ophthalmol Vis Sci. 2004; 45:4352–4358. [PubMed: 15557443]

May CA. Comparative anatomy of the optic nerve head and inner retina in non-primate animal models used for glaucoma research. Open Ophthalmol J. 2008; 2:94–101. [PubMed: 19516911]

Moore CG, et al. Long-term non-invasive measurement of intraocular pressure in the rat eye. Curr Eye Res. 1995; 14:711–717. [PubMed: 8529407]

Moore CG, et al. Circadian rhythm of intraocular pressure in the rat. Curr Eye Res. 1996; 15:185–191. [PubMed: 8670727]

Moore CG, et al. Noninvasive measurement of rat intraocular pressure with the Tono-Pen. Invest Ophthalmol Vis Sci. 1993; 34:363–369. [PubMed: 8440590]

Morrison J, et al. Structure and composition of the rodent lamina cribrosa. Exp Eye Res. 1995a; 60:127–135. [PubMed: 7781741]

Morrison JC. Elevated intraocular pressure and optic nerve injury models in the rat. J Glaucoma. 2005; 14:315–317. [PubMed: 15990616]

Morrison JC, et al. Pathophysiology of human glaucomatous optic nerve damage: insights from rodent models of glaucoma. Exp Eye Res. 2011; 93:156–164. [PubMed: 20708000]

Morrison JC, et al. Limbal microvasculature of the rat eye. Invest Ophthalmol Vis Sci. 1995b; 36:751–756. [PubMed: 7890506]

Morrison JC, et al. Reliability and sensitivity of the TonoLab rebound tonometer in awake Brown Norway rats. Invest Ophthalmol Vis Sci. 2009; 50:2802–2808. [PubMed: 19324849]

Morrison JC, et al. Rat models for glaucoma research. Prog Brain Res. 2008; 173:285–301. [PubMed: 18929117]

Morrison JC, et al. Understanding mechanisms of pressure-induced optic nerve damage. Prog Retin Eye Res. 2005; 24:217–240. [PubMed: 15610974]

Morrison JC, et al. Microvasculature of the rat optic nerve head. Invest. Ophthalmol. Vis. Sci. 1999; 40:1702–1709. [PubMed: 10393039]

Morrison JC, et al. A rat model of chronic pressure-induced optic nerve damage. Exp Eye Res. 1997; 64:85–96. [PubMed: 9093024]

Norman RE, et al. Dimensions of the human sclera: Thickness measurement and regional changes with axial length. Exp Eye Res. 2010; 90:277–284. [PubMed: 19900442]

Pang IH, Clark AF. Rodent models for glaucoma retinopathy and optic neuropathy. J Glaucoma. 2007; 16:483–505. [PubMed: 17700292]

Ren R, et al. Lamina cribrosa and peripapillary sclera histomorphometry in normal and advanced glaucomatous Chinese eyes with various axial length. Invest Ophthalmol Vis Sci. 2009; 50:2175–2184. [PubMed: 19387083]

Rosner, B. 12.9. The Intraclass Correlation Coefficient, Fundamentals of Biostatistics. Seventh Edition ed.. Harvard University. Brooks/Cole Cengage Learning; Boston, MA: 2011. p. 569

Ruiz-Ederra J, Verkman AS. Mouse model of sustained elevation in intraocular pressure produced by episcleral vein occlusion. Exp Eye Res. 2006; 82:879–884. [PubMed: 16310189]

Sigal IA, et al. Factors influencing optic nerve head biomechanics. Invest. Ophthalmol. Vis. Sci. 2005; 46:4189–4199. [PubMed: 16249498]

Sigal IA, et al. 3D morphometry of the human optic nerve head. Exp Eye Res. 2010; 90:70–80. [PubMed: 19772858]

Sugiyama K, et al. Optic nerve and peripapillary choroidal microvasculature in the primate. J Glaucoma. 1994; 3(Suppl 1):S45–54. [PubMed: 19920587]

Sugiyama K, et al. Optic nerve and peripapillary choroidal microvasculature of the rat eye. Invest. Ophthalmol. Vis. Sci. 1999; 40:3084–3090. [PubMed: 10586928]

Yang H, et al. 3-D histomorphometry of the normal and early glaucomatous monkey optic nerve head: prelaminar neural tissues and cupping. Invest Ophthalmol Vis Sci. 2007a; 48:5068–5084. [PubMed: 17962459]

Yang H, et al. Physiologic intereye differences in monkey optic nerve head architecture and their relation to changes in early experimental glaucoma. Invest Ophthalmol Vis Sci. 2009a; 50:224–234. [PubMed: 18775866]

Yang H, et al. 3-D histomorphometry of the normal and early glaucomatous monkey optic nerve head: lamina cribrosa and peripapillary scleral position and thickness. Invest Ophthalmol Vis Sci. 2007b; 48:4597–4607. [PubMed: 17898283]

Yang H, et al. Deformation of the normal monkey optic nerve head connective tissue after acute IOP elevation within 3-D histomorphometric reconstructions. Invest Ophthalmol Vis Sci. 2009b; 50:5785–5799. [PubMed: 19628739]

Yang H, et al. Deformation of the early glaucomatous monkey optic nerve head connective tissue after acute IOP elevation in 3-D histomorphometric reconstructions. Invest Ophthalmol Vis Sci. 2011; 52:345–363. [PubMed: 20702834]

Highlights

- This is the first 3D characterization of rat optic nerve head (ONH) anatomy.
- Unlike the primate the rat ONH consists of superior and inferior scleral openings.
- The rat optic nerve is surrounded by a vascular plexus within the superior canal.
- Bruch's Membrane extends into the superior canal to abut the superior nerve.
- Three posterior ciliary artery branches create an irregular inferior scleral canal.

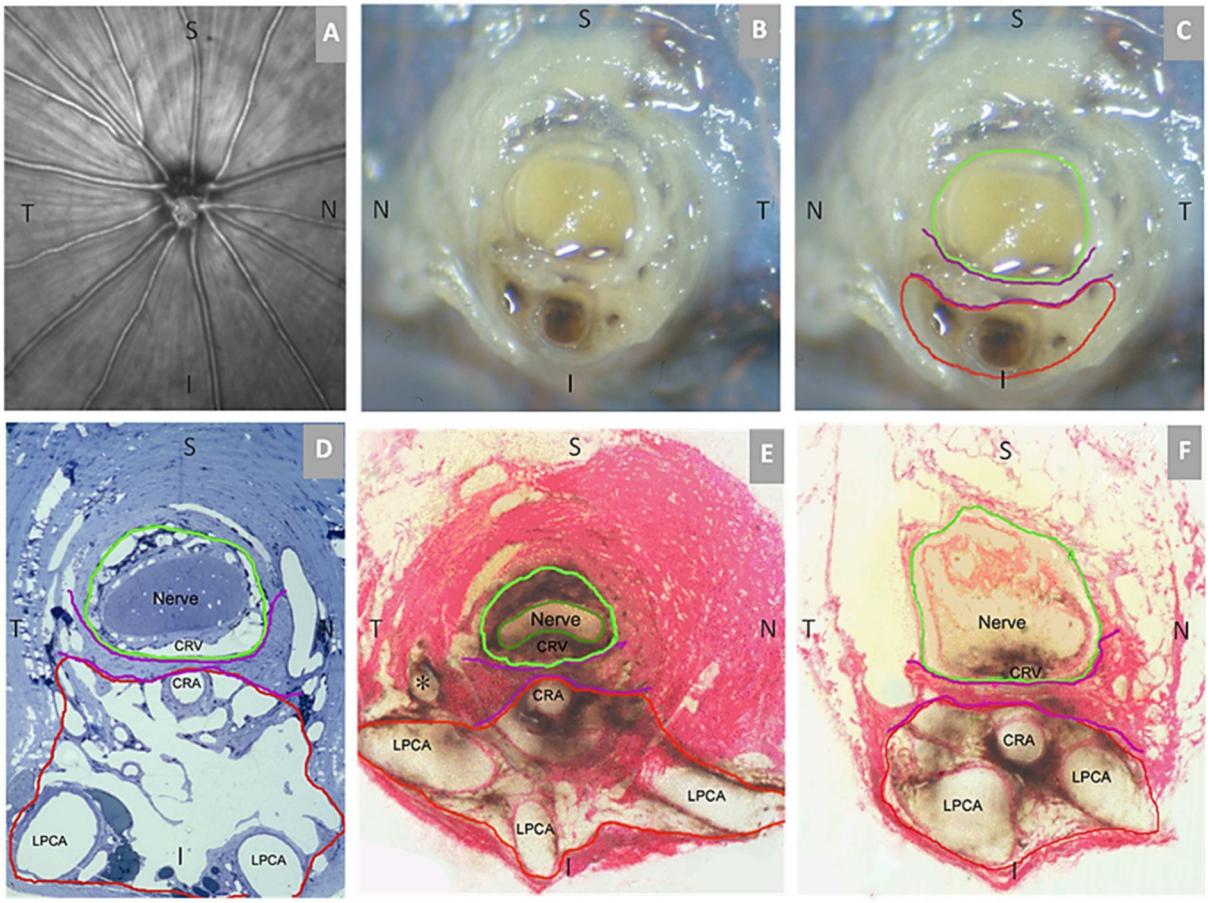

Figure 1. Rat Optic Nerve Head Macroscopic and Microscopic Relationships I – Transverse Sections

(A) 30 degree SDOCT Infrared Reflectance image of the rat optic disc (the vitreal surface of the optic nerve head) (courtesy of Brad Fortune). **(B)** Macroscopic appearance of the cut surface of the rat optic nerve just posterior to the scleral shell (view from the back of the eye). **(C)** Principal macroscopic relationships: 1) the **neurovascular bundle (green)**; and the more-inferior **2) arterial bundle (red)**; are separated by a sling of scleral tissues **3) the scleral sling, (purple)** (view from the back of the eye). **(D-E)** Principal scleral openings. Unlike the primate, there are two principal openings within the sclera of the rat ONH: 1) the neurovascular canal (green) and the more-inferior arterial opening (red), which is not a well-defined canal, being irregular due to the choroidal branches of the LPCAs (D and E) and separated from the neurovascular canal by the scleral sling (purple). Unlike the primate, which has on average 15 short posterior ciliary arteries that are evenly distributed around the circumference of the scleral canal, the inferior concentration of the LPCAs and the density of their intrascleral branches to the choroid combined with the actual CRA canal (D – F) suggest an “effective” second opening in the sclera. (D) Transverse histologic section through the scleral portion of the optic nerve head demonstrating the same relationships seen posterior to the globe in panels B and C. Note that the neurovascular bundle consists of the optic nerve surrounded by a vascular plexus within the inferior portion of which runs the CRV. The arterial bundle is made up of the central retinal artery, the two main LPCAs and

their intrascleral branches to the choroid (vascular spaces in between the principal arteries - not labeled). (E) A digital transverse section image from a histomorphometric reconstruction demonstrating the same relationships as (D). (F) Digital section image from the same eye just posterior to the globe and close to the view seen macroscopically in (C). The intrascleral (E) and retrobulbar short posterior ciliary arteries (F) are branches of the LPCAs rather than the Ophthalmic Artery. A preferential superior-temporal course of the optic nerve and neurovascular bundle as they pass through the sclera into the orbit are suggested by comparing the green circle in (F) to (E). CRV- Central retinal vein, LPCAs- Long Posterior Ciliary Arteries. N – Nasal; T – Temporal; I –Inferior; S – Superior.

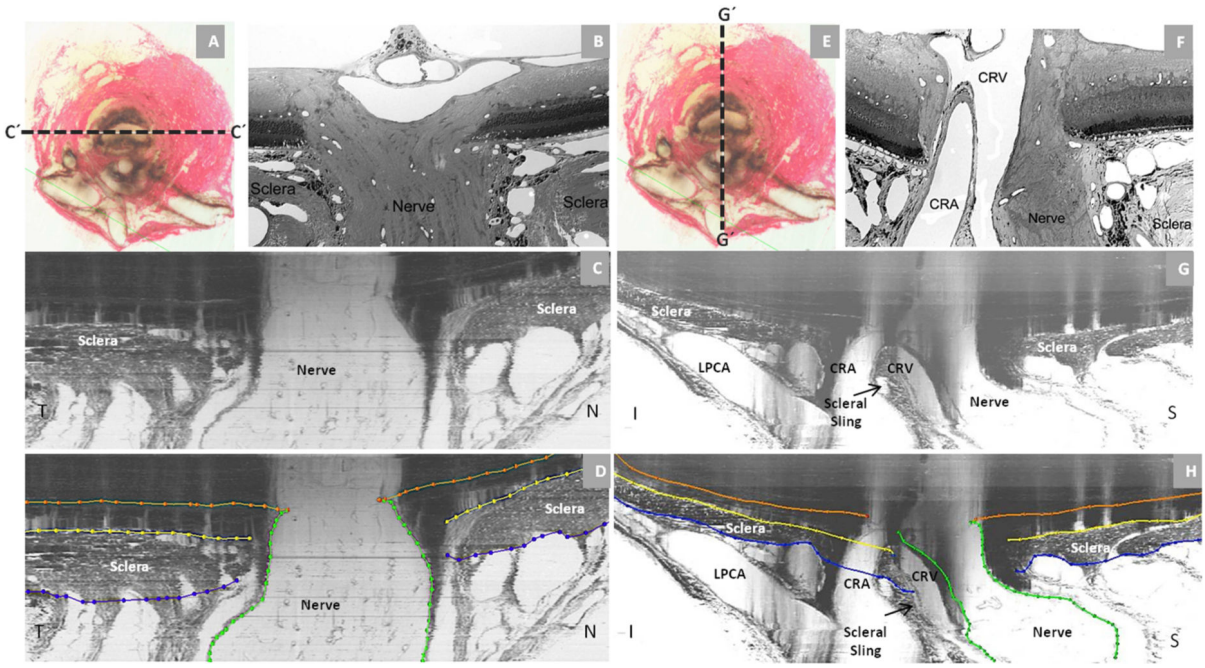

Figure 2. Rat Optic Nerve Head Macroscopic and Microscopic Relationships II

Horizontal (panels - **A**, **B**, **C** and **D**) and vertical (panels - **E**, **F**, **G** and **H**) sagittal views of the rat ONH centered upon the scleral portion of the neurovascular canal (A and E). Panels (C) and (G) are digital horizontal and vertical sagittal sections (location relative to the ONH marked as C' and G' in (A) and (E) of the same histomorphometric reconstruction in which acquired transverse section images were shown in Figure 1. Panels D and H are the same sections showing the delineation of the different structures. The process of creating digital radial sagittal sections from the histomorphometric volume is explained in Figure 3, below. Panels (B) and (F) are histologic sections of another eye acquired in locations similar to (C) and (G). Note the continuity of the choroidal and perineural vascular plexus within both sections. Most published descriptions of the rat ONH show horizontal (C) or vertical (G) sagittal sections of the ONH that are cropped close to the end of the sclera which has the effect of emphasizing the similarities of the neurovascular canal to the scleral canal of the primate. However within the horizontal (C) and vertical (G) digital sagittal sections of the histomorphometric reconstructions, the importance of the vascular plexus that surrounds the nerve within the neurovascular canal, the sclera sling and the inferior arterial vessels can be appreciated. Note also the general temporal slant of the nerve in (B) and the superior slant of the nerve in (F). Taken together, these observations within horizontal and vertical sagittal sections confirm the general superior temporal path of the optic nerve tissues suggested within the serial transverse section images of Figure 1 (see Figure legend). Note that within panels (C) and (G) of Figure 2, the dark shadows extending upward from the sclera are a result of the fact that in serial transverse sectioning from the vitreous (top) to the orbital optic nerve (bottom) the dark choroidal pigment can be seen until the sectioning plane passes through it, creating the appearance of a shadow within the retina and vitreous . CRV-Central retinal vein, LPCA- Long Posterior Ciliary Arteries. CRA-Central Retinal Artery; N – Nasal; T – Temporal; I – Inferior; S – Superior.

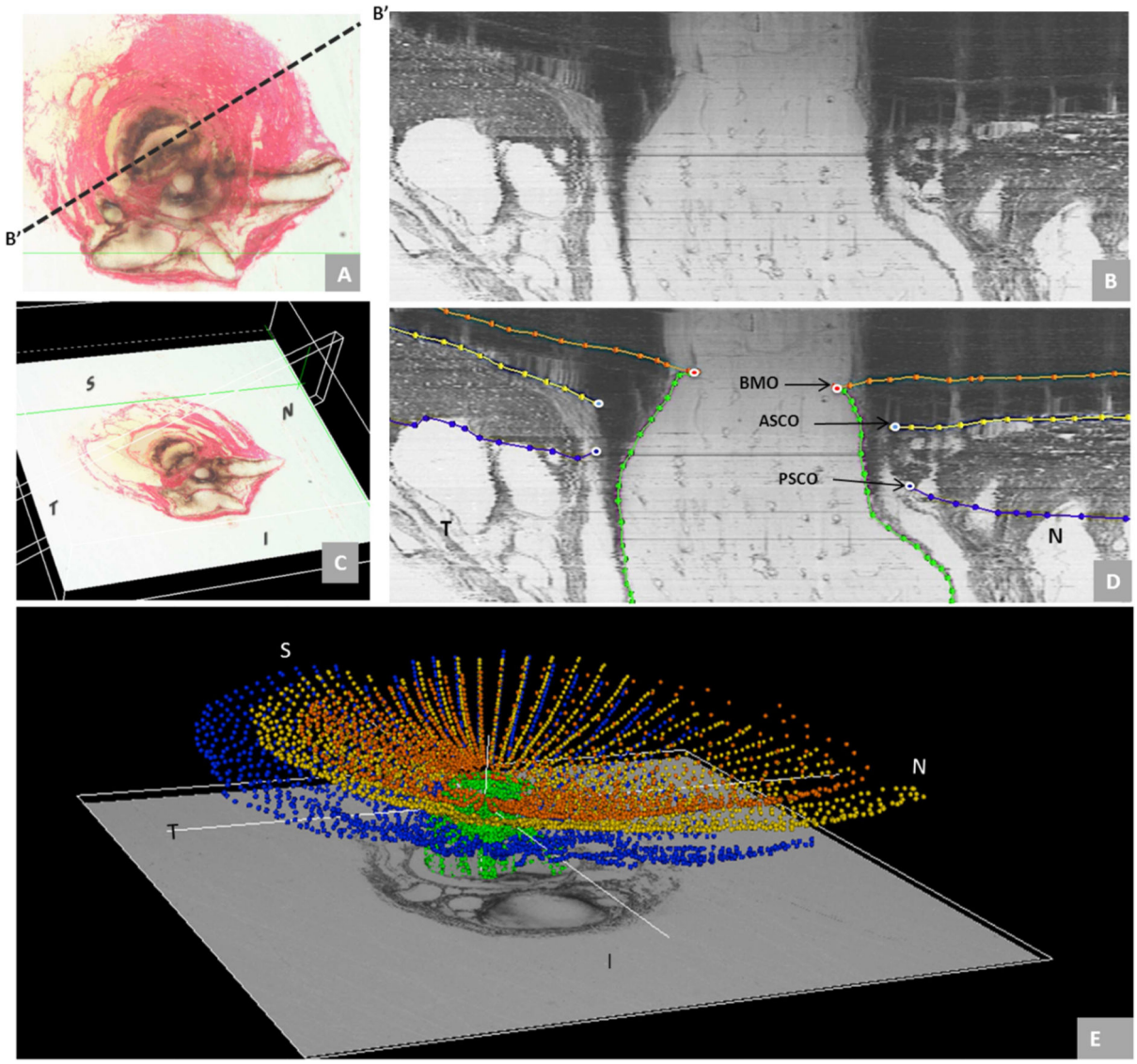

Figure 3. 3D Delineation of the ONH and Peripapillary Scleral Landmarks

Delineated landmark points within 40 digital radial sagittal section images of a representative ONH. The delineator first assigned the center of the scleral portion of the optic nerve (A) to be the center of rotation through which, forty, 7-voxel thick, digital radial sagittal section images (B) of the digital 3D reconstruction (C) were serially served at 4.5° intervals. The Nasal-Temporal location of (B) is shown here two dimensionally (dotted line marked B'-B') within the transverse section image in (A) and three-dimensionally (7 μm thick white-edged rectangle) within the 3D reconstruction in (C). Within each digital sagittal section image (B) the delineator marked four landmark surfaces and three pairs of neurovascular canal landmarks (one point on each side of the canal). The landmark surfaces were: (1) Bruch's membrane (orange); (2) the anterior (yellow) and (3) posterior (blue) surfaces of peripapillary sclera ; and (4) the optic nerve boundary extending from Bruch's membrane opening, through the scleral canal and along the pia mater to the posterior edge of the reconstruction (green). The landmark points were Bruch's Membrane Opening (BMO –

red), the anterior scleral canal opening (ASCO – light blue) and the posterior scleral canal opening (PSCO – purple). A representative point cloud which contains all delineated landmark types for all 40 radial sections of an individual reconstruction is viewed from its superior surface three dimensionally in (D) (nasal is to the left and temporal is to the right). Three dimensional reconstructions of the landmark point clouds (D) of each eye were 3D visualized together and separately (turning each landmark category on and off) so as to qualitatively determine their principal macroscopic relationships. In Panel (E) the superior course of the optic nerve (outlined by green dots) as it passes through the sclera and its sharper bend into the orbit can be appreciated. N – Nasal; T – Temporal; I – Inferior; S – Superior.

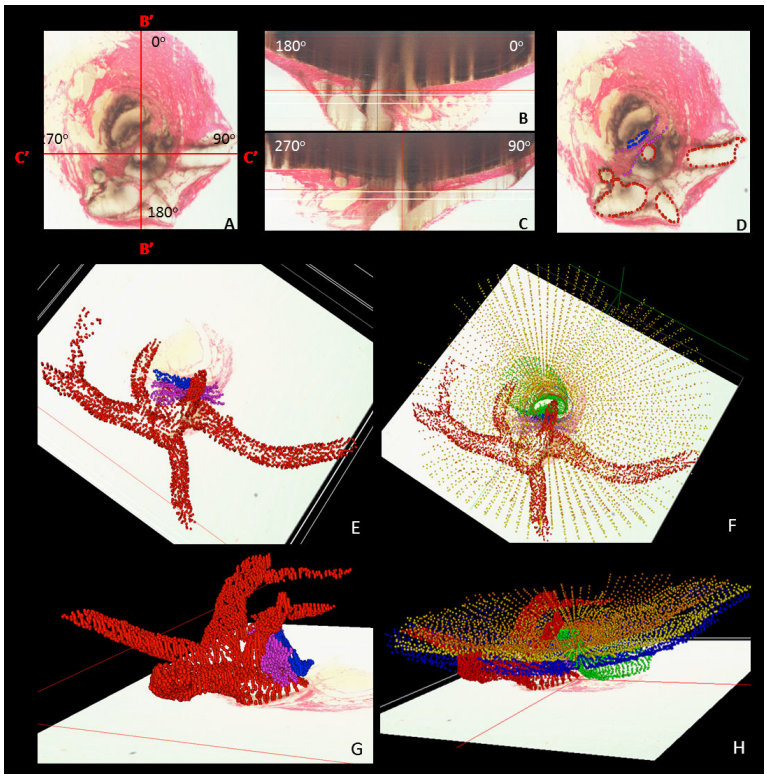

Figure 4. 3D Delineation of the ONH and Peripapillary Scleral Vasculature and Scleral Sling within Digital Transverse Section Images

Vessel and scleral sling delineation were performed within every fourth digital transverse section image (A) while simultaneously viewing one linked window which displayed either embedded vertical (B) or embedded horizontal (C) digital sagittal sections through the point being delineated. The lines marked B'-B' and C'-C' in panel (A) mark the location of the embedded vertical and embedded horizontal digital sagittal section images depicted in panel (B) and (C), respectively. Note that these are vertical and horizontal sections through the 3D reconstruction, but because the tissues are not embedded in perfect clinical orientation, they are not "anatomic" vertical and horizontal sections through the ONH. In Figure 2, this same reconstruction has been turned so that an accurate clinical orientation has been achieved and "anatomic" vertical and horizontal sections are shown. The following landmark categories were individually marked and catalogued within each delineated transverse section image (D): Ophthalmic artery (OA - red); (2) Central retinal artery (CRA - red);(3) Long posterior ciliary arteries (LPCA - red); (4) Short posterior ciliary arteries (SPCA – reds – and branches of the LPCAs in rats); (5) Central retinal vein (CRV - blue); and (6) the vascular or neural boundary of the scleral sling (magenta). Three dimensional reconstructions of the landmark point clouds (panels E - H) were then 3D visualized together and separately (turning each landmark category on and off) so as to determine their principal macroscopic relationships.

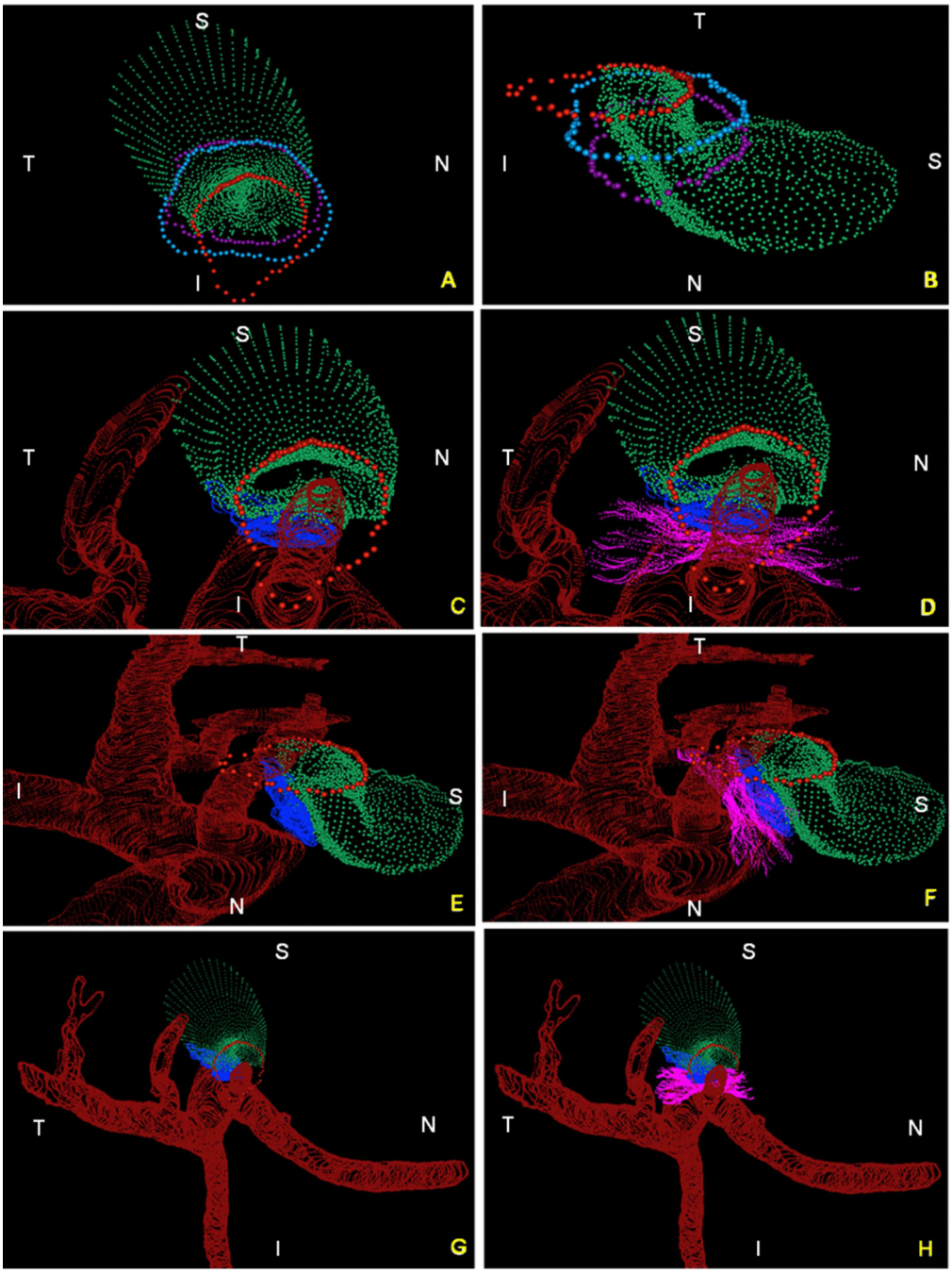

Figure 5. Summary of the 3D relationships between BMO, the ASCO and PSCO, the Optic Nerve, the Central Retinal Vein, the Central Retinal Artery and the Long Posterior Ciliary Arteries (with and without their intrascleral branches) as visualized within the 3D Point Clouds from a Representative Normal Rat Eye

The relationship of BMO (red), ASCO (light blue) and PSCO (purple) relative to the optic nerve (green) can be seen from a clinical orientation in panel (A) and longitudinally in panel (B). In panels (C) - (F) the ASCO and PSCO Point clouds have been turned off and the CRV, CRA and LPCA point clouds have each been turned on. First, notice that BMO is not round (A) but inferiorly elongated to accommodate the passage of the CRA and CRV (blue

vessel) to the retina. Notice also, that BMO is shifted inferiorly relative to the ASCO and PSCO. Second, notice the space between the neural tissue and the BMO, ASCO and PSCO in panel (B). At the level of BMO, the nerve abuts BM superiorly and there is space inferior to the nerve (filled by the CRV and CRA) as noted above. Note in Panel B, that because of the shift in BMO relative to the ASCO and PSCO, BM effectively extends beyond the scleral portion of the neural canal. Superiorly this creates an edge or extension of BM against which the neural bundle abuts. Inferiorly, it creates an elongation of BMO to accommodate the inferior vessels. The net effect of this shift is to create a superior-directed, oblique passage of the nerve through the wall of the rat eye that is best appreciated in Panels B, E and F. At the level of its passage through the anterior (ASCO) and posterior (PSCO) sclera the nerve is surrounded by a vascular plexus which we are not able to independently delineate using our current method. Third, there are three long posterior ciliary arteries which branch from the CRA behind the globe and pass together through the sclera (inferior to the neurovascular canal) to achieve the choroid. Their tangential rather than perpendicular passage through the sclera is depicted in (E) and (F) (see also Figure 4F, 4H and Figure 7). Fourth, short posterior ciliary arteries (defined to be primary branches of the ophthalmic artery that individually pass through the sclera) were not identified. Instead the few arteries that independently pass through the sclera superiorly (G), where identified, appear to be retrobulbar branches of the LPCAs. Fifth, unlike the primate eye in which there are 15 short posterior ciliary arteries that are relatively equidistant from one another around the circumference of the optic nerve, the choroidal blood supply in the rat appears to originate inferiorly from a dense plexus of intrascleral LPCA branches which effectively fill the space between the three LPCA branches (see Figure 1D – 1F). Some of these vessels extend within the sclera and choroid superiorly, around the neurovascular canal. It is the density of the LPCAs and their intrascleral branches inferiorly that suggests an “effective”second opening in the sclera. Sixth, the CRA and CRV are separated from each other and the nerve proper and supported by a “sling”(magenta) of scleral tissues that forms the inferior border of the neurovascular scleral canal opening and the superior border of the more-inferior arterial opening. N – Nasal; T – Temporal; I – Inferior; S – Superior.

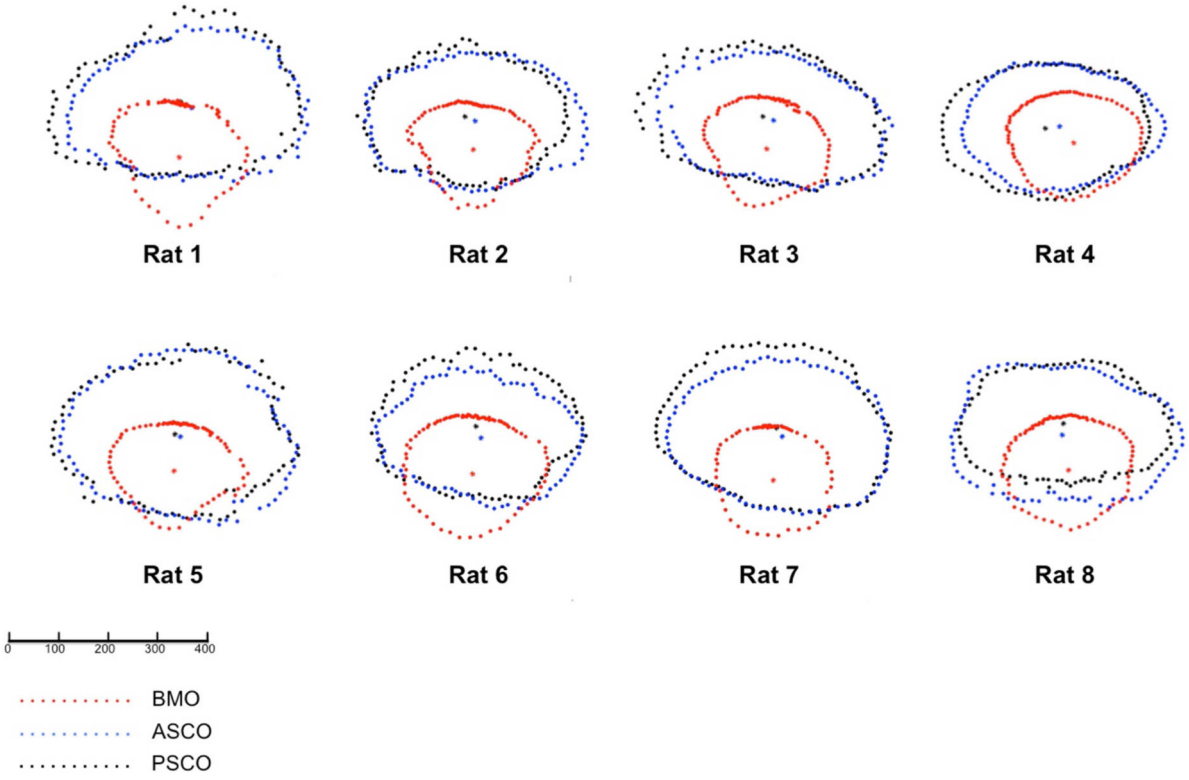

Figure 6. Eye-specific comparisons of BMO (red), ASCO (blue) and PSCO (black) for the 8 normal control eyes

All data are in right eye configuration. Delineated points for each structure along with their centroid are superimposed by projection to the BMO reference plane for comparison purposes. These data suggest the extent to which BMO is shifted inferiorly relative to the ASCO and PSCO for all 8 study eyes. Combined with the oblique course of the optic nerve bundle visualized in Figure 9, above, these data provide anatomic support for the oblique course of the nerve from BMO through the PSCO, the superior extension of BM (and inferior shift of BMO) relative to the ASCO and PSCO, and the physical abutment of RGC axons against BMO superiorly in the rat ONH. The scale is in micrometers.

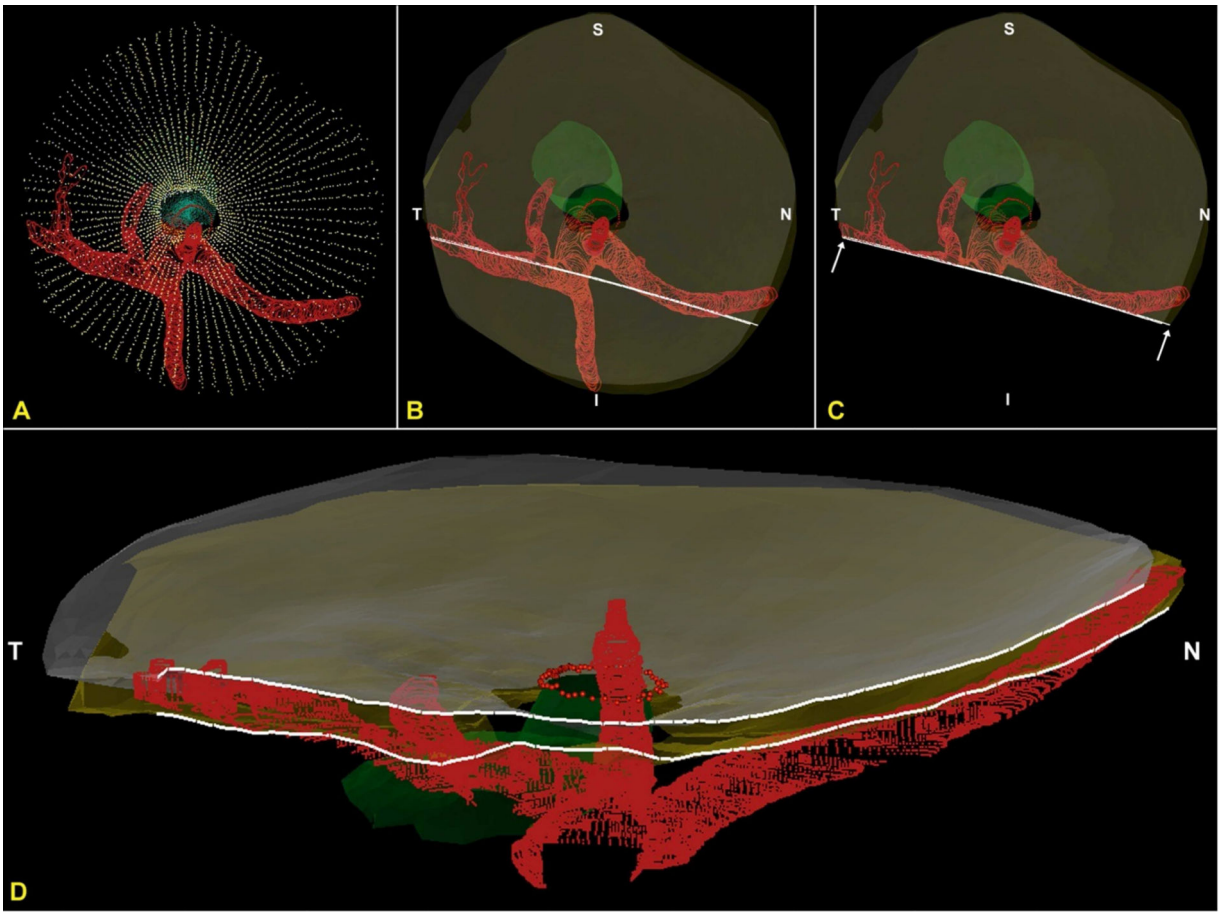

Figure 7. The CRA passes perpendicularly and the LPCAs pass obliquely through the arterial scleral opening (views from the anterior or vitreal surface)

(A) Standard Point cloud 3D reconstruction showing the scleral openings, nerve and BMO (B) The anterior and posterior scleral surface point clouds from the ONH in (A) have been transparently surfaced. Dark transparent circles correspond to the scleral openings and the nerve is transparent green, BMO is shown with red dots (C) A digital section through portions of both the nasal and temporal LPCAs has been removed and its cut surface is visualized in (D). Note that the inferior LPCA is, in this eye, a branch of the temporal LPCA (B). The temporal LPCA (left in B and D) enters the sclera near the CRA opening and slowly achieves the choroidal space well away from the ONH. The nasal LPCA (right in Band D) takes an even more gradual course through the sclera. In most eyes, the space between the LPCAs and the CRA contains choroidal branches from the LPCA which can be very dense (Figure 1D – 1F). Finally, note the general superior and temporal passage of the nerve (transparent green) relative to the dark scleral canal openings and (red) inferior arterial tree (Panels B and C) N – Nasal; T – Temporal; I – Inferior; S – Superior.

Table 1

Abbreviations and Definitions table

Abbreviation	Meaning
ANOVA	Analysis of Variance
ASCO	Anterior Scleral Canal Opening
BM	Bruch's Membrane
BMO	Bruch's Membrane Opening
CI	Confidence Interval
CRA	Central Retinal Artery
CRV	Central Retinal Vein
Eye-specific results	Parameters related to an individual eye
GLS	Generalized Least Squares
H/V	Horizontal/Vertical Ratio
I	Inferior
ICC	Intraclass Correlation Coefficient
IOP	Intraocular Pressure
LPCA	Long Posterior Ciliary Artery
N	Nasal
NA	Not Available or Not Applicable
OA	Ophthalmic Artery
OD	Right Eye
ON	Optic Nerve
ON-ASCO	Optic Nerve area at the level of ASCO
ON-PSCO	Optic Nerve area at the level of PSCO
ONH	Optic Nerve Head
OS	Left Eye
Overall results	Global parameters (all rats together)
PSCO	Posterior Scleral Canal Opening
S	Superior
SD	Standard Deviation
SPCA	Short Posterior Ciliary Artery
T	Temporal

Table 2

Animal and Eye Data

No.	ID	Age at sacrifice (months)	Eye	Mean IOP (mmHg)	Number of Digital Serial Section Images
1	MR8	9.5	OD	28.5	400
2	MR10	9.5	OS	28.8	313
3	MR1	9.5	OS	28.3	398
4	MR9	9.5	OS	28.4	307
5	MR12	10.5	OS	28.5	275
6	MR11	10.5	OS	28.3	375
7	MR5	9.5	OD	28.8	484
8	MR4	9.5	OD	28.4	501

No.- Rat number for this Study; ID – Laboratory Rat Identification Number; Eye - OD-Right eye, OS-left eye; Mean IOP (mmHg)- Mean IOP of all IOP measurements taken AM and PM for each eye; Number of Digital Serial Section Images- number of digital serial section images required to reconstruct each optic nerve head.